

Origin of dips and peaks in the absolute fully resolved cross sections for the electron-impact double ionization of He

A. Lahmam-Bennani,¹ I. Taouil,¹ A. Duguet,¹ M. Lecas,¹ L. Avaldi,² and J. Berakdar³

¹*Laboratoire des Collisions Atomiques et Moléculaires, UMR 8625 Bâtiment 351, Université Paris XI, F-91405 Orsay Cedex, France*

²*IMAI del CNR, Area della Ricerca, Casella Postale 10, 00016 Monterotondo Scalo, Italy*

³*Max-Planck Institut für Mikrostrukturphysik, Weinberg 2, 06120 Halle, Germany*

(Received 10 November 1998)

Using a multiparameter multicoincidence spectrometer, we have measured the coplanar ($e,3e$) angular distributions following the double ionization of helium at an incident energy of ≈ 5.6 keV and under a small projectile's scattering angle of 0.45° . The two ejected electrons have been detected with equal energies $E_b = E_c = 10$ eV. The absolute value of the cross section is determined with an accuracy of 25%. The origin of dips and peaks in the spectra is exposed by analyzing the corresponding theoretical calculations. These calculations have been done using a four-body final-state wave function for the three electrons moving in the field of He^{2+} . The dipolar limit is investigated and the manifestation of the deviation from this limit are pointed out. General features and possible trends for other targets are proposed. [S1050-2947(99)02805-X]

PACS number(s): 34.80.Ht, 34.80.Dp

I. INTRODUCTION

Recently, there has been an increased activity in the study of the double ionization (DI) processes under photon or electron impact. This progress has been fueled by the spectacular advances in the development of very sophisticated, high sensitivity new spectrometers [1–5] that render possible the energy and angle-resolved simultaneous detection of two or three final-state electrons. Thus, in such measurements the energy and momentum transferred to the target, the energies and momenta of all the final-channel electrons are simultaneously determined. Apart from the spin degrees of freedom these measurements yield, in the case of the He target, the ultimate information obtainable on the collision dynamics and provide hence the most sensitive probe for theoretical approaches. The challenge and promise in the theoretical investigations of these processes lie in the modeling and understanding of the inherently nonseparable many-body interacting systems (in the case of electron impact DI, the final state consists of three electrons moving in the field of He^{2+}) and in the treatment of the particular difficulties associated with the infinite range of the Coulomb potentials.

The ideal target for such a goal is helium, as it is the simplest two-electron system, and the electron impact double ionization, the so-called ($e,3e$) collision, leads to a pure four-body problem in the final state. In the last few years, the one-photon double-ionization experiments have provided a wealth of new results in several kinematics and for several rare gas targets [e.g., [6] and references quoted therein]. In contrast, the ($e,3e$) experiments [7] have proved much more difficult to perform. Detailed ($e,3e$) experiments have been recently reported for the outer-shell DI of argon [8] and neon [9], hereafter referred to as I and II, respectively. However, due to the low triple coincidence counting rate, the modest energy resolution used in I and II on the fast electron channel did not allow us to distinguish among different final states of the doubly charged ion. Therefore, in that sense, these were

not kinematically completely determined experiments. In this paper we report a determination of the ($e,3e$) cross sections for DI of He, obtained in absolute units (a subset of the data was published in [10]). For the first time, a kinematically completely determined experiment has been performed, since the He^{2+} ion is a bare nucleus with no relevant internal structure. These experiments are the follow-up of our research program aimed at elucidating the relative importance of the various DI mechanisms under electron impact, see I and II. The results of these measurements are analyzed in light of theoretical calculations using a correlated four-body final state wave function and employing initial state wave functions of various quality. The origin of dips and peaks as well as the relative heights of the peaks is well understood from certain rules that are valid in the optical regime. The validity of the optical limit is investigated and the contribution of nondipolar terms to the cross sections are unraveled. The absolute value of the cross sections turns out to be very sensitive to the used initial states. Throughout this paper, atomic units are used and the same notation as in I is used. In particular, positive angles are measured counterclockwise, starting from the incident beam direction.

II. EXPERIMENT

The experimental setup and procedure are identical to those reported in I, see also [1]. Briefly, the incident electron, labeled 0, and the three outgoing electrons, indexed a for the fast “scattered” one and b and c for the two slow “ejected” ones are all detected in the same plane. The impact energy is $E_0 \approx 5.6$ keV. The scattered electron (e_a) is observed at a fixed angle, $\theta_a = +0.45^\circ$, and is energy analyzed in a 127° cylindrical analyzer. The two ejected electrons (e_b and e_c) have identical energies, $E_b = E_c = 10$ eV. They are selected in two opposite half planes with respect to the electron beam in dual double toroidal electrostatic analyzers, and are separately detected by two position sensitive multidetection systems (PSDMDS), each constituted by three multichannel

plates and a resistive anode. The angular information contained in the collision plane ($\mathbf{k}_0, \mathbf{k}_a$), i.e., the ejection angles θ_b and θ_c , is preserved upon arrival on the PSDs due to the focusing properties of toroidal analyzers. To register triple coincidence events, two identical time-to-amplitude converters are used, both simultaneously started by the same pulse from detector a , and, respectively, stopped by the b - and c -electron pulses. For each triple coincidence event, the arrival positions on the PSDs of the e_b and e_c electrons are recorded and stored in a specially dedicated computer, together with their arrival times with respect to e_a . All further treatment of the data is done in the off-line analysis, see [1]. For these experiments, the whole spectrometer was carefully realigned, and a special emphasis was placed on (i) optimizing the transmission of all the electron optics, (ii) maximizing the three detectors efficiencies, and (iii) minimizing contributions from extraneous electrons. This was strongly needed since the helium DI cross section is appreciably smaller than the one for argon or for neon targets. As a result, the efficiency increased by a factor of 3 as compared to the studies I and II. Yet, the true triple coincidence count rate was only two counts per hour. Hence, to achieve a reasonable statistical error, a long accumulation time is needed, a total of 33 days of continuous, nonstop acquisition for all the data presented in this paper. Due to this long accumulation time and to a local, rather high noncoincident count rate on each detector assembly, the data had to be corrected for the MCPs local fatigue effect, described in I. The correction is typically less than 10% and never exceeds 20%.

The ($e, 3e$) relative cross sections are measured by fixing all the kinematical parameters: The incident electron energy is chosen as $E_0 = 5599$ eV. The scattered electron energy and angle are $E_a = 5500$ eV and $\theta_a = +0.45^\circ$, respectively. This corresponds to a momentum transfer $K = 0.24$ a.u. The ejected electron energies are $E_b = E_c = 10$ eV. In the off-line analysis, the total angular range subtended by each PSD ($20-160^\circ$ and $200-340^\circ$, respectively, for θ_b and θ_c) is divided into ten sectors, each $\pm 7^\circ$ width, and the data are subsequently depicted for a fixed θ_b as a function of varying θ_c . The method used for the absolute scale determination is basically the same as in I. It relies on the measurement of double and triple differential cross sections (DDCS and TDCS, respectively) for He under the same kinematical parameters as in the ($e, 3e$) experiments, and their comparison with known theoretical values. The main (but obvious) difference with I is that it is not necessary anymore to compare Ar and He DDCS as done in I, so that Eq. (5) of I simplifies into (see I for the notation),

$$\sigma_{abc} = f_{abc} \frac{\sigma_a^{(\text{He BR})}}{f_a^{(\text{He BR})}} \frac{\sigma_{ab}^{(\text{He OCW})}}{f_{ab}^{(\text{He})}} \frac{\sigma_{ac}^{(\text{He OCW})}}{f_{ac}^{(\text{He})}} \times \sqrt{\frac{\Delta E_a^2 + \Delta E_b^2 + \Delta E_c^2}{(\Delta E_a^2 + \Delta E_b^2)(\Delta E_a^2 + \Delta E_c^2)}}. \quad (1)$$

The immediate consequence is a better final accuracy in the absolute scale determination, estimated here to be 25%.

III. THEORETICAL CONSIDERATIONS

The probability for the three final-channel electrons a, b, c to be detected, respectively within solid angles of apertures $d\Omega_a, d\Omega_b, d\Omega_c$, and energies E_a, E_b and E_c is related to

$$\frac{d^5\sigma}{d\Omega_a d\Omega_b d\Omega_c dE_b dE_c} = (2\pi)^4 \frac{k_a k_b k_c}{k_0} |T_{fi}|^2, \quad (2)$$

where E_a is then determined from energy conservation. The transition matrix element T_{fi} is given by

$$T_{fi} = \langle \Psi_{\mathbf{k}_a, \mathbf{k}_b, \mathbf{k}_c}(\mathbf{r}_a, \mathbf{r}_b, \mathbf{r}_c) | W | \Phi(\mathbf{r}_a, \mathbf{r}_b, \mathbf{r}_c) \rangle, \quad (3)$$

where $\mathbf{r}_a, \mathbf{r}_b, \mathbf{r}_c$ are the position vectors of the projectile and the two initially bound electrons, respectively, and $\mathbf{k}_a, \mathbf{k}_b, \mathbf{k}_c$ are the corresponding conjugate momenta. The state vectors $|\Phi(\mathbf{r}_a, \mathbf{r}_b, \mathbf{r}_c)\rangle$ and $|\Psi_{\mathbf{k}_a, \mathbf{k}_b, \mathbf{k}_c}(\mathbf{r}_a, \mathbf{r}_b, \mathbf{r}_c)\rangle$ in Eq. (3) represent the four-body system (three electrons in the field of He^{2+}) in the initial and final state, respectively, and W is the perturbation due to which the double ionization occurs. For the initial state we choose the unperturbed representation

$$\Phi_i(\mathbf{r}_a, \mathbf{r}_b, \mathbf{r}_c) = (2\pi)^{-2/3} \exp(\mathbf{k}_0 \cdot \mathbf{r}_a) \varphi(\mathbf{r}_b, \mathbf{r}_c), \quad (4)$$

with $\varphi(\mathbf{r}_b, \mathbf{r}_c)$ being the ground-state wave function of He. The wave function (4) is an eigensolution of the Hamiltonian H_i with an eigenvalue E_i where $E_i = k_0^2/2 - \epsilon$ with $\epsilon \approx 2.9037$ a.u. being the (positive) binding energy of $\text{He}(^1S^e)$. The Hamiltonian H_i has the form

$$H_i = H_0 - \frac{Z_T}{r_b} - \frac{Z_T}{r_c} + \frac{1}{|\mathbf{r}_b - \mathbf{r}_c|}, \quad (5)$$

where H_0 is the total kinetic energy operator and $Z_T = 2$ is the charge of He^{2+} . Thus, the total Hamiltonian of the system can be written as

$$H = H_i - \frac{Z_T}{r_a} + \frac{1}{|\mathbf{r}_a - \mathbf{r}_b|} + \frac{1}{|\mathbf{r}_a - \mathbf{r}_c|}. \quad (6)$$

According to the standard scattering theory [11], the perturbation W in Eq. (3) derives to

$$W = H - H_i = -\frac{Z_T}{r_a} + \frac{1}{|\mathbf{r}_a - \mathbf{r}_b|} + \frac{1}{|\mathbf{r}_a - \mathbf{r}_c|}. \quad (7)$$

The state vector $|\Psi_{\mathbf{k}_a, \mathbf{k}_b, \mathbf{k}_c}(\mathbf{r}_a, \mathbf{r}_b, \mathbf{r}_c)\rangle$ is an eigenstate of H with an eigenenergy,

$$E = k_a^2/2 + k_b^2/2 + k_c^2/2 + k_{\text{ion}}^2/2M = E_0 - \epsilon, \quad (8)$$

where \mathbf{k}_{ion} is the recoil momentum of He^{2+} and M is the mass of the alpha particle. Consequently, one has to resort to approximate procedures to obtain useful expressions for $|\Psi\rangle$.

Recently, a strategy has been proposed [12,13] to derive approximate wave functions for N interacting continuum particles. The resulting wave function is a product of $N(N-1)/2$ (in our case 6) two-body Coulomb waves. Each of them represents a specific, Coulomb interacting two-body subsystem. Unfortunately, in general, even this (simple) approximation is intractable for practical applications (at lower incident energies a full computational approach has been

presented in Refs. [14,15]). Therefore, for the present case of two slow and one fast electrons moving in the double continuum of He^{+2} , it has been suggested to completely subsume the interaction of the fast electron with all other particles into effective electron-nucleus interactions of the slow electrons.

To this end we employ the same ideas as in Ref. [13]. Defining $r_{ij} = \mathbf{r}_i - \mathbf{r}_j$, $i, j \in \{a, b, c\}$, we write the total potential as

$$-\frac{Z_T}{r_a} - \frac{Z_T}{r_b} - \frac{Z_T}{r_c} + \frac{1}{r_{ab}} + \frac{1}{r_{ac}} + \frac{1}{r_{bc}} = \frac{Z_b}{r_b} + \frac{Z_c}{r_c} + \frac{Z_{bc}}{r_{bc}}, \quad (9)$$

with Z_b, Z_c, Z_{bc} being functions yet to be determined. A way of specifying these functions is to linearly expand in terms of the two-body interactions, as done in Ref. [12] and require Eq. (9) to be identically fulfilled. In addition, the asymptotic limits, as described in Ref. [12] have to be satisfied. Such a procedure yields under the assumption $r_j \propto k_j$, $j = a, b, c$,

$$\begin{aligned} Z_b &= -Z_T - \frac{Z_T k_b}{2 k_a} + \frac{k_b}{|\mathbf{k}_a - \mathbf{k}_b|}, \\ Z_c &= -Z_T - \frac{Z_T k_c}{2 k_a} + \frac{k_c}{|\mathbf{k}_a - \mathbf{k}_c|}, \\ Z_{bc} &= 1. \end{aligned} \quad (10)$$

With these effective charges the eigenfunction $|\Psi\rangle$ of H can be approximated by [12]

$$\Psi_{\mathbf{k}_a, \mathbf{k}_b, \mathbf{k}_c}(\mathbf{r}_a, \mathbf{r}_b, \mathbf{r}_c) \approx (2\pi)^{-3/2} \exp(i\mathbf{k}_a \cdot \mathbf{r}_a) \psi,$$

where

$$\begin{aligned} \psi &= (2\pi)^{-3} N \exp(i\mathbf{k}_b \cdot \mathbf{r}_b + i\mathbf{k}_c \cdot \mathbf{r}_c) {}_1F_1(i\alpha_{bc}, 1, -i[k_{bc}r_{bc} \\ &+ \mathbf{k}_{bc} \cdot \mathbf{r}_{bc}]) {}_1F_1(i\alpha_b, 1, -i[k_b r_b + \mathbf{k}_b \cdot \mathbf{r}_b]) \times {}_1F_1(i\alpha_c, 1, \\ &-i[k_c r_c + \mathbf{k}_c \cdot \mathbf{r}_c]). \end{aligned} \quad (11)$$

The normalization factor is

$$\begin{aligned} N &= \exp(-\pi\alpha_{bc}/2) \Gamma(1 - i\alpha_{bc}) \exp(-\pi\alpha_b/2) \Gamma(1 - i\alpha_b) \\ &\times \exp(-\pi\alpha_c/2) \Gamma(1 - i\alpha_c). \end{aligned}$$

Here the effective Sommerfeld parameters have been defined as $\alpha_c = Z_c/k_c$, $\alpha_b = Z_b/k_b$, and $\alpha_{bc} = Z_{bc}/(2k_{bc})$, where \mathbf{k}_{bc} is the momentum conjugate to \mathbf{r}_{bc} .

Combining Eq. (3) and Eq. (7), the scattering amplitude T_{fi} can be written as the sum of three scattering amplitudes:

$$\begin{aligned} T_{fi} &= T_a + T_{ab} + T_{ac} = \left\langle \Psi \left| \frac{-Z}{r_a} \right| \Phi \right\rangle + \left\langle \Psi \left| \frac{1}{|\mathbf{r}_a - \mathbf{r}_b|} \right| \Phi \right\rangle \\ &+ \left\langle \Psi \left| \frac{1}{|\mathbf{r}_a - \mathbf{r}_c|} \right| \Phi \right\rangle. \end{aligned} \quad (12)$$

The amplitudes T_a , T_{ab} , T_{ac} describe the *direct* scattering of the projectile electron from the nucleus and the two electrons, respectively. In addition, the state vector $|\Psi\rangle$ contains multiple scatterings within the four-body system as final-state interaction.

Within the present model, T_{fi} depends dynamically on all vectors $\mathbf{k}_0, \mathbf{k}_a, \mathbf{k}_b, \mathbf{k}_c$, as clearly seen from Eqs. (10) and (11). In fact, if the projectile electron approaches, in velocity space, one of the ejected electrons, say, electron b , the interaction of this ejected electron with the nucleus turns repulsive [i.e., Z_b , as defined by Eq. (10) becomes positive) as to simulate the repulsion between the scattered and the ejected electron b .

In the first Born approximation (FBA), on the other hand, one replaces the total Hamiltonian H [Eq. 6] by H_i [16]. Thus initial and final-state wave functions become solutions of the same Hamiltonian H_i for different eigenvalues and thus the term T_a in Eq. (12), i.e., the direct scattering from the nucleus, vanishes since it contains a direct overlap of the initial and the final state. Within the FBA the structure of the wave function $|\Psi_{\mathbf{k}_a, \mathbf{k}_b, \mathbf{k}_c}(\mathbf{r}_a, \mathbf{r}_b, \mathbf{r}_c)\rangle$ is the same as in Eq. (11); however, the effective charges in Eqs. (10) reduce to $Z_b = -Z = Z_c$, $Z_{bc} = 1$. The amplitude T_{fi} depends then only on three vectors \mathbf{k}_b , \mathbf{k}_c and the momentum transfer $\mathbf{K} = \mathbf{k}_0 - \mathbf{k}_a$. For small K the amplitude T_{fi} can be Taylor expanded in K , which leads to the optical limit,

$$T_{fi} = -iK \langle \psi_{\mathbf{k}_b, \mathbf{k}_c}(\mathbf{r}_b, \mathbf{r}_c) | \hat{\mathbf{K}}(\mathbf{r}_b + \mathbf{r}_c) | \varphi(\mathbf{r}_b, \mathbf{r}_c) \rangle + O(K^2). \quad (13)$$

Thus, to the first order in K the dipole matrix element (13) is proportional to the transition amplitude for double photoionization by linearly polarized light. The electric-field vector is pointing into the \mathbf{K} direction. We remark here that within the optical limit final and initial states are always orthogonal because only the odd-parity part of the final state contributes to the matrix element, and this odd-parity final state is automatically orthogonal to the even initial state.

For the subsequent discussion it is important to note that Eq. (13) is an expansion in K only. For a fixed K , the dynamical matrix element in Eq. (13) depends very much on the scattering geometry, i.e., on \mathbf{k}_b and \mathbf{k}_c . This means that for a fixed K the optical limit might be approached for certain combination of \mathbf{k}_b and \mathbf{k}_c but violated for other \mathbf{k}'_b and \mathbf{k}'_c , as we will see below.

IV. RESULTS AND DISCUSSION

For the computation of the cross section (2) we employ the wave function (11) for the final state. The ground state of He is represented by a Slater wave function,

$$\varphi_s(\mathbf{r}_b, \mathbf{r}_c) = N_s \exp[-Z_s(r_b + r_c)], \quad (14)$$

or alternatively a Hylleraas-type wave function [17],

$$\begin{aligned} \varphi_h(\mathbf{r}_b, \mathbf{r}_c) &= N_h [\exp(-C_b r_b - C_c r_c + C_{bc} r_{bc}) \\ &+ \exp(-C_c r_b - C_b r_c + C_{bc} r_{bc})], \end{aligned} \quad (15)$$

where N_s and N_h are normalization factors and $Z_s, C_j, j \in b, c, bc$ are variational parameters used to minimize the binding energy. In addition, we compare with the results obtained by approximating T_{fi} by the dipole term in Eq. (13).

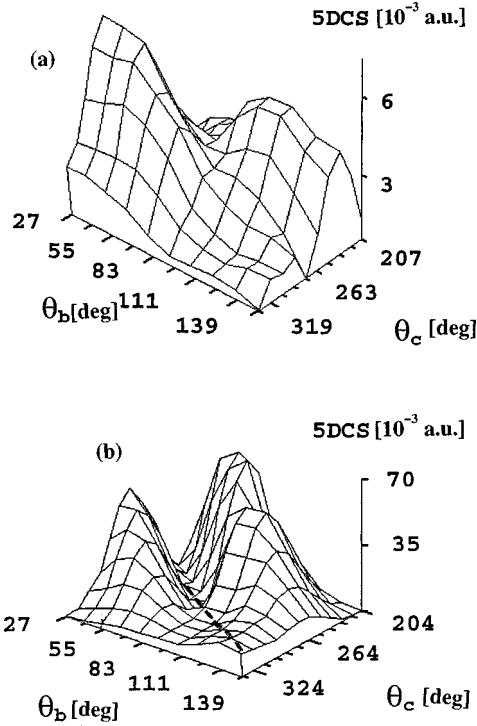


FIG. 1. Three-dimensional plot of the measured absolute ($e,3e$) fivefold differential cross section for helium, versus the ejection angles θ_b and θ_c . The scattering angle of the fast electron is fixed $\theta_a = +0.45^\circ$. The incident energy is 5.6 keV. The ejected electrons are detected with equal energies $E_b = E_c = 10$ eV. The absolute experimental data (a) are depicted along with the theoretical results (b) as calculated using Eqs. (11) and (15). The dashed line in (b) corresponds to the minimum momentum imparted to the ion.

The absolute experimental data are shown in Fig. 1(a) as a function of the polar ejection angles θ_b and θ_c .¹ Correspondingly, the theoretical results are depicted in Fig. 1(b). One notices that the electrons c and b are preferentially emitted in two groups that appear as two “hills” in Figs. 1(a) and 1(b), mostly arranged about $(\theta_b = 115^\circ, \theta_c = 237^\circ)$ for the first group, called backward group, and about $(\theta_b = 45^\circ, \theta_c = 275^\circ)$ for the second one, called forward group. (Forward and backward are meant with respect to the incident direction, the forward half-plane being defined by $0 < \theta_b < 90^\circ$ and $\theta_c > 270^\circ$, and the backward half-plane being defined by $90^\circ < \theta_b < 180^\circ$ and $180^\circ < \theta_c < 270^\circ$.) When compared to corresponding scattering geometry for argon and neon targets (respectively, Fig. 5 of I and Fig. 2 of II), a trend can be observed when going from the lighter to the heavier atom. Though in the three cases, the emission of both electrons in the backward half-plane is dominant, one observes in He a significant forward emission of both electrons, almost equal in intensity to the backward one. This forward emission is relatively less important in neon and is practically absent in argon where the cross section is largely dominated by the backward emission.

For the interpretation of the present findings, we recall

¹The full set of data can be obtained upon request from A. Lahmam-Bennani. Electronic address: azzedine@ferrari.lcam.u-psud.fr

that in a previous study [18] it has been anticipated that structures in the ($e,3e$) cross section can be linked to the recoil momentum \mathbf{k}_{ion} , where

$$\mathbf{k}_{\text{ion}} = \mathbf{k}_0 - \mathbf{k}_a - \mathbf{k}_b - \mathbf{k}_c. \quad (16)$$

In the present experiment, the energies E_j and momenta $k_j = \sqrt{2E_j}$, $j \in \{0, a, b, c\}$ are measured, so that k_{ion} is deduced straightforward from Eq. (16) (the binding energy ϵ enters in Eq. (16) via the energy conservation law).

In analogy to electron-impact single ionization it has been argued [18] that the cross section should be maximal when the momentum \mathbf{K} imparted by the projectile is very small and directly and completely absorbed by the two-ejected electrons, i.e., when $k_{\text{ion}} = 0$, the kinematical conditions under which this is the case have been termed “Bethe sphere.” This prediction cannot be substantiated by the present experimental and theoretical study. In fact, the “hills” in Figs. 1(a) and 1(b) correspond to a large k_{ion} (cf. also Fig. 3). The reason for this apparent contradiction is the following. For fast-glancing collisions the optical limit (13) is approached. The optical transition (13) is, however, forbidden for two “free” electrons, which is the condition for the “Bethe sphere,” i.e., for photon absorption without participation of the nucleus. This is because a photon imparts to the system energy but basically no momentum; therefore, the electrons must recoil off the massive nucleus.

While the predictions of Ref. [18] for the maxima in the cross section are not confirmed [cf. Fig. 1(a) and Fig. 1(b)], the positions anticipated for the minima in case of $E_0 \gg \epsilon$, $K \ll 1$ are well confirmed and provide a useful tool to interpret the data. These minima occur when: (a) $\mathbf{k}_b = -\mathbf{k}_c$ because in this case the amplitude T_{fi} is proportional to K^{2n} and n is a positive integer, i.e., the leading dipole term vanishes, (b) $\hat{\mathbf{k}}_b \perp \mathbf{K}$ and $\hat{\mathbf{k}}_c \perp \mathbf{K}$ as the dipole term is zero, and (c) $\mathbf{k}_b = \mathbf{k}_c$ due to electronic repulsion. In addition, we remark here that an additional minimum appears if (d) $(\mathbf{k}_b + \mathbf{k}_c) \perp \mathbf{K}$ since the optical transition is forbidden in this case (cf. Ref. [19] and references therein). All the minima listed above turn to zero points for optical transitions [19–21].

To clearly show that the positions of the minima are confirmed by the experiment we scan the angular distributions of one of the electrons, say, electron b while the other ejected electron is detected under a fixed angle θ_c . The positions of the minima listed above are indicated by arrows labeled a , b , c , and d corresponding to the minima (a), (b), (c), and (d).

The results are depicted in Figs. 2(a)–2(t). The general trend and *shape* of the distribution is reasonably described by the theory with different representations of the initial state; however, as for the magnitude of the cross sections, large differences between theory and experiment are observed. In addition, the absolute value of the cross section is highly sensitive to the initial-state description. A possible explanation of this behavior is given below.

In some cases the ($e,3e$) cross sections reveal obvious deviations from the optical cross section as calculated according to Eq. (13) [cf. Figs. 2(f)–2(j) and Figs. 2(q)–2(t)]. However, in most cases the optical limit seems to be reached in this geometry (and within the present model). The reason for the deviations from the optical limit will be discussed below.

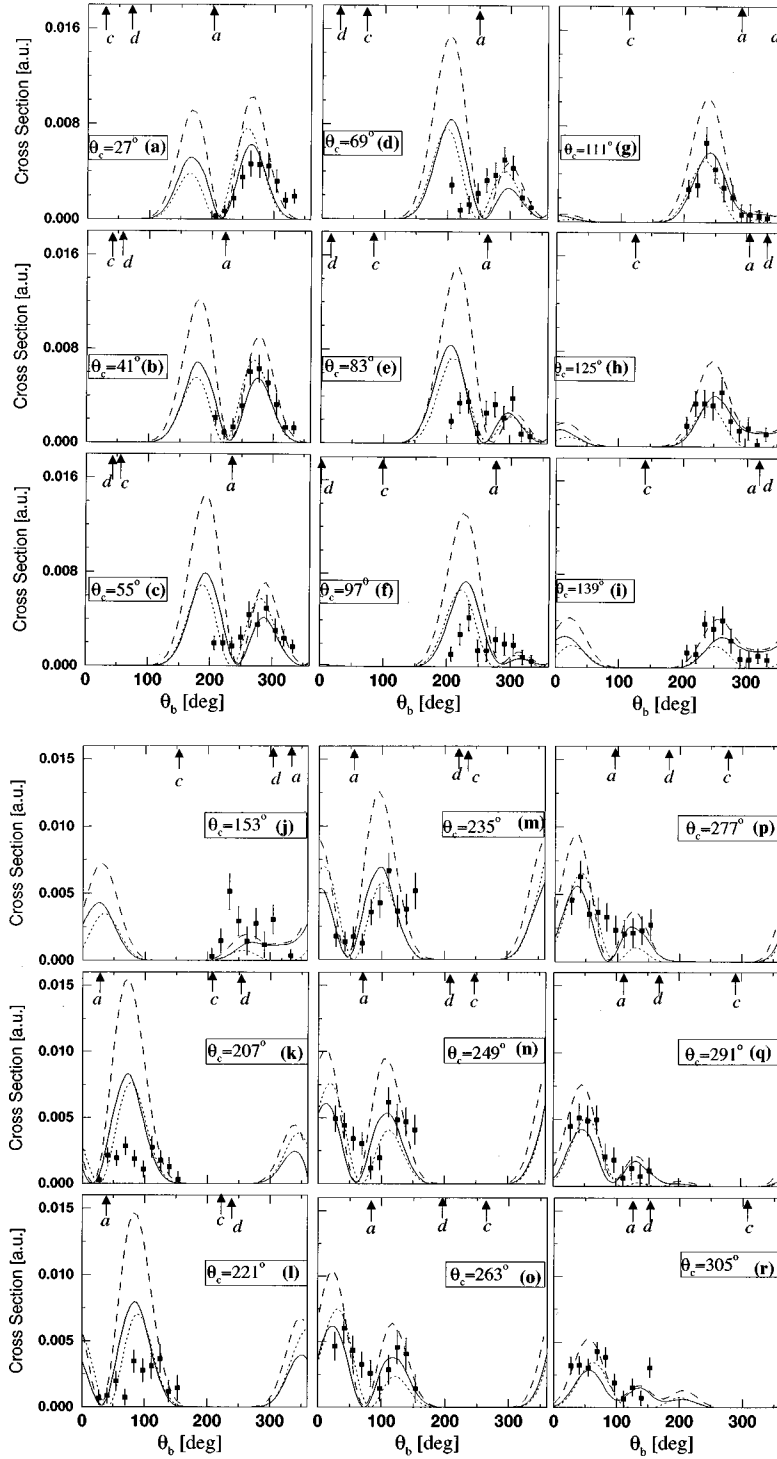


FIG. 2. For the same scattering geometry as in Fig. 1, the angular distribution of one of the electrons (electron b) is scanned while the other ejected electron is detected under a fixed angle θ_c . The angle θ_c is indicated on the figures. The arrows labeled a, c, d mark the angular positions of, respectively, the minima (\mathbf{a}), (\mathbf{c}), (\mathbf{d}) as determined in the text. The geometrical arrangement for the minimum (\mathbf{d}) is illustrated in Fig. 2(u). The normal to \mathbf{K} is denoted by \mathbf{N} . The momentum transfer vector \mathbf{K} is indicated. Using Eqs. (11) and (15) leads to the solid curve. The dotted curve is the results in the optical limit (13). The solid and dotted curves have been scaled down by a factor of 10 for comparison. The dashed curve is the result for the $(e, 3e)$ cross section when using Eqs. (11) and (14).

At first it is important to analyze the seemingly complicated metamorphosis of the cross section as θ_c varies between the situations in Fig. 2(a) and Fig. 2(t).

To this end we remark that the angular positions of the minima (the zero points for photon impact) $\mathbf{a}, \mathbf{b}, \mathbf{c}, \mathbf{d}$, as listed above, are, respectively,

$$(a) k_b \cos \theta_b = -k_c \cos \theta_c,$$

$$(b) k_0 \cos \theta_b - k_a \hat{\mathbf{k}}_a \cdot \hat{\mathbf{k}}_b = 0 \text{ and } k_0 \cos \theta_c - k_a \hat{\mathbf{k}}_a \cdot \hat{\mathbf{k}}_c = 0,$$

$$(c) k_c \cos \theta_c = k_b \cos \theta_b,$$

$$(d) k_b(k_0 \cos \theta_b - k_a \hat{\mathbf{k}}_a \cdot \hat{\mathbf{k}}_b) = -k_c(k_0 \cos \theta_c - k_a \hat{\mathbf{k}}_a \cdot \hat{\mathbf{k}}_c).$$

The angular position of the minimum (\mathbf{d}) is illustrated in

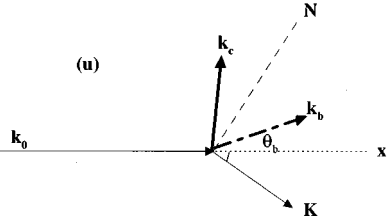
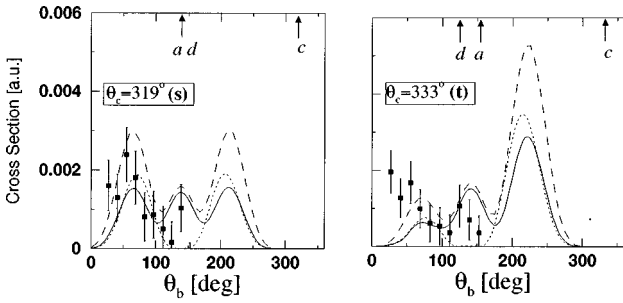


FIG. 2. (Continued).

Fig. 2(u). As $E_b = E_c$ the vectors \mathbf{k}_b and \mathbf{k}_c must be positioned symmetrically with respect to an axis normal to $\hat{\mathbf{K}}$ [axis \mathbf{N} in Fig. 2(u)].

Inspecting Figs. 2(a)–2(t) with regard to the positions of these minima (indicated by arrows labeled correspondingly), it is apparent that the shape of the cross section is basically determined by those minima except for the cases where $(e,3e)$ cross sections differ substantially from photoionization cross sections [cf. Figs. 2(f)–2(j) and Figs. 2(q)–2(t)]. The characteristic two-lobe structure can also be explained: Since $E_b = E_c$, the photo-ionization cross sections possess the following symmetry properties.

(i) For $\hat{\mathbf{k}}_c = \pm \hat{\mathbf{K}}$ (i.e., for $\theta_c \approx 139^\circ$ and for $\theta_c = 319^\circ$), the angular distribution, as depicted in Figs. 2(a)–2(t) must be cylindrically symmetric with respect to $\hat{\mathbf{K}}$. This is the case in Figs. 2(i) and 2(s).

(ii) For $\hat{\mathbf{K}} \cdot \hat{\mathbf{k}}_c = 0$, (i.e., for $\theta_c \approx 49^\circ$ and for $\theta_c \approx 229^\circ$) the angular distribution of electron b possess reflection symmetry with respect to an axis normal to $\hat{\mathbf{K}}$ (this is due to the fact that the polarization vector for linearly polarized photon enters bilinearly in the photoionization cross section, i.e., it defines an axis rather than a vector). This condition is approximately approached in Figs. 2(b), 2(c), 2(l), and 2(m).

The combinations of these symmetry properties and the above positions of the minima allow for an angular distribution with three lobes. This maximal case is observed in Fig. 2(q).

Having established that the two lobes in Figs. 2(i) and 2(s) and Figs. 2(b), 2(c), 2(m), and 2(l) have to be of roughly the same magnitudes due to symmetry requirements (i) and (ii), respectively, the diminishing size of the lobe located around $\theta_b > 300^\circ$ in the intermediate cases depicted in Figs. 2(c)–2(h) can be assigned to the minimum (d) passing through this lobe. Same observations are made for Figs. 2(j)–2(t).

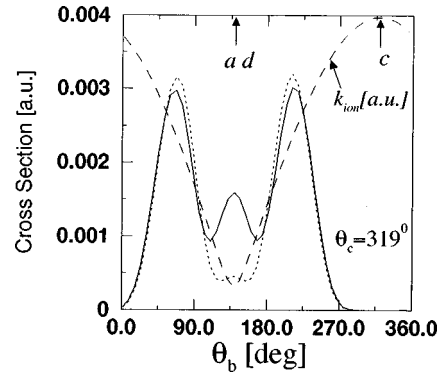


FIG. 3. The scattering geometry is that of Fig. 2(s) with the solid curve being the results when employing Eqs. (11) and (14). If we keep $E_c = E_b = 10$ eV and θ_c , θ_b as in Fig. 2(s) but increase E_0 to $E_0 = 20.1$ keV and choose $\theta_a = 0.12^\circ$, we end up with the results shown by the dotted curve scaled down by a factor of 4. The dashed curve is $k_{\text{ion}}(\theta_b)$, as given by Eq. (16) scaled down by a factor of 400.

In fact, tracing the movement of the position of the minimum (d) as θ_c changes, the bouncing ratio of the magnitudes of the two lobes is nicely explained.

In Figs. 2(f)–2(j) and 2(q)–2(t) one notices considerable deviations from the optical limits, e.g., the minima (a, d) are not present in the $(e,3e)$ cross sections. These differences seem to be compatible with experiment. In fact, a more obvious violation of the optical limit has been observed when presenting the data as a function of the mutual angle θ_{bc} [10] (i.e., adding up all the pairs that have the same θ_{bc} , irrespective of the directions $\hat{\mathbf{k}}_b$, $\hat{\mathbf{k}}_c$).

These deviations are due to the contributions of higher-order multipoles in the expansion (13). For a fixed K (as in Fig. 2) the contributions of these multipoles to the series (13) depend dynamically on the scattering geometry, i.e., on \mathbf{k}_b and \mathbf{k}_c . This leads to the behavior observed in Fig. 2, i.e., for a fixed K the validity of the optical limit is very much dependent on the geometrical arrangement of \mathbf{k}_b and \mathbf{k}_c . It should be noted, however, that with diminishing K the limit (13) is approached and the contributions of the higher-order multipoles are suppressed. This is illustrated in Fig. 3 where we have chosen the scattering geometry of Fig. 2(s) as a prototype example. In Fig. 3 we keep the position of $\hat{\mathbf{K}}$ fixed but reduce K from $K = 0.24$ [in Figs. 2(a)–2(t)] to $K = 0.124$. The momenta \mathbf{k}_b and \mathbf{k}_c are the same as in Fig. 2(s). This can be achieved by increasing the incident energy to $E_0 = 20.099$ keV and reducing the scattering angle to 0.12° . As clearly seen in Fig. 3 the $(e,3e)$ cross section approaches the photoionization cross section due to the decreased K and the small “hill” around $\theta_b = 139^\circ$ diminishes.

That the optical limit is not reached does not logically imply that the $(e,3e)$ cross section should show a maximum at the position where the photoionization cross section vanishes ($\theta_b = 139^\circ$). The reason for the small “hill” in the $(e,3e)$ cross section around $\theta_b = 139^\circ$ is immediately clear if we consider the angular distribution of k_{ion} , as given by Eq. (16). Exactly at $\theta_b = 139^\circ$, the position of the “hill,” k_{ion} is minimal, i.e., the momentum transferred to the two-electron subsystem is maximal. This is the original definition of the Bethe sphere as given in the previous work [18].

To come back to the beginning of our discussion, we argued that the $(e,3e)$ cross section near the Bethe sphere is suppressed by the minima $\mathbf{a}-\mathbf{d}$, which seems to have higher priority than the Bethe-sphere maxima. However, if those restrictive minima are released, for reasons of geometry and/or not approaching the optical limit, the maxima due to the Bethe-sphere condition show up. We performed the same calculations, as those shown in Fig. 3, for the cases where deviations from photoionization cross sections are considerable and came to the conclusion that, as above, the recoil momentum k_{ion} is minimal when $(e,3e)$ diverges markedly from the photoionization cross sections.

It should be noted here that for all cases of Figs. 2(a)–2(t) the momentum transfer $K=0.24$ a.u. is the same. Thus, we can generally state that (within our model) approaching the optical limit is not a question of the magnitude of K only but depends sensitively on the scattering geometry, i.e., the dynamic contained in the matrix elements in the expansion (13).

Having established that the deviations of the $(e,3e)$ cross sections from the photoionization cross sections are the signature of nondipolar contributions and recalling that Eq. (13) is only valid within the FBA, we can now consider the situations where the FBA is not expected to perform well and hence the optical limit breaks down. With regard to this aspect, two points can be noted.

(1) As stated above, the projectile scattering from the nucleus, as described by the amplitude T_a , vanishes within the FBA. Hence, a considerable T_a (with respect to T_{ab}, T_{ac}) signifies deviations from the FBA and consequently the break of the cylindrical symmetry associated with $\hat{\mathbf{K}}$ and the optical limit. On the other hand, T_a increases with increasing Z_T [cf. Eq. (12)]; thus, the break of symmetry around $\hat{\mathbf{K}}$ and the violation of the optical limit should be more prevalent for heavier targets. In fact, such a behavior has already been observed for argon and neon (papers I and II).

(2) As mentioned above, the FBA is obtained from the present model in the special case $Z_b = -Z_T = Z_c$, $Z_{bc} = 1$ of Eq. (10). Therefore, as can be deduced from Eq. (10), the deviations from the optical limit and the violation of the symmetry associated with the FBA are expected to enhance with increasing E_b and/or E_c , in particular for higher Z_T .

As for the absolute magnitude of the cross section the theoretical results using the simple initial state (14) are more or less in the range of the experimental findings. In contrast, the theory employing the initial state (15) yields results an order of magnitude higher than the experimental cross sec-

tions. It turned out that the reason for this surprising result is that the direct overlap between the initial and the final states $\langle \Psi | \Phi \rangle$ is much bigger for the wave function (15) than for Eq. (14). On the other hand the term $\langle \Psi | \Phi \rangle$ indicates the amount of spurious transitions in absence of any perturbations or when the perturbation is small. It should be stressed in this context that while minimizing the term $|\langle \Psi | \Phi \rangle|$ is desirable, a negligible $|\langle \Psi | \Phi \rangle|$ does not say much as to the quality of the wave functions Ψ and Φ , as demonstrated in this paper. It means merely that the same approximations have been made in deriving Φ and Ψ regardless of the quality of these approximations. Of course, an exact description of Ψ and Φ leads to vanishing overlap $|\langle \Psi | \Phi \rangle|$.

One might think of orthogonalizing the initial and the final state as done in Ref. [18]. However, as stressed in Ref. [18], one obtains a spurious term in the orthogonalized wave functions.

In light of these remarks it seems useful to search for a wave function Φ that yields not only the best possible value for the ground-state energy but also minimizes the term $|\langle \Psi | \Phi \rangle|$.

V. CONCLUSIONS

We have reported kinematically completely determined $(e,3e)$ experiments for helium. The improved sensitivity of the experimental setup enabled us to extract a full set of angular distributions. The absolute magnitudes of the measured angular distributions have been determined with an accuracy of 25%. The measured data are compared with theoretical calculations that employ a four-body state in the exit channel. The origin of the structures observed in the angular correlation pattern has been exposed and the range of validity of the dipolar limit has been envisaged. Deviations from the optical limits have been assigned to higher-order multipoles that are dynamically dependent on the scattering geometry. It has been demonstrated that the contributions of these multipoles diminish at very small momentum transfer. Moreover, we argued that nondipolar contributions are more pronounced for stronger Coulomb fields of the residual ion as well as for higher energies of the ejected electrons. Deviations between experiment and theory as far as the absolute value is concerned have been traced back to a spurious direct overlap between initial and final states used in this study. This shortcoming is due to the use of different approximations in the initial and final states when deriving the initial- and final-state wave functions.

[1] A. Duguet, A. Lahmam-Bennani, M. Lecas, and B. El Marji, *Rev. Sci. Instrum.* **69**, 3524 (1998).
 [2] M. J. Ford, J. P. Doering, J. H. Moore, and M. A. Coplan, *Rev. Sci. Instrum.* **66**, 3137 (1995).
 [3] H. Kollmus, W. Schmitt, R. Moshhammer, M. Unverzagt, and J. Ullrich, *Nucl. Instrum. Methods Phys. Res. B* **124**, 377 (1997).
 [4] T. J. Reddish, G. Richmond, G. W. Bagley, J. P. Wightman, and S. Cvejanovic, *Rev. Sci. Instrum.* **68**, 2685 (1997).

[5] J. Mazeau, P. Lablanquie, P. Selles, L. Malegat, and A. Huetz, *J. Phys. B* **30**, L293 (1997).
 [6] R. Dörner, J. Feagin, C. L. Cocke, H. Bräuning, O. Jagutzki, M. Jung, E. P. Kanter, H. Khemliche, S. Kravis, V. Mergel, M. H. Prior, H. Schmidt-Böcking, L. Spielberger, J. Ullrich, M. Unverzagt, and T. Vogt, *Phys. Rev. Lett.* **77**, 1024 (1996).
 [7] A. Lahmam-Bennani, C. Dupré, and A. Duguet, *Phys. Rev. Lett.* **63**, 1582 (1989).

- [8] B. El Marji, C. Schröter, A. Duguet, A. Lahmam-Bennani, M. Lecas, and L. Spielberger, *J. Phys. B* **30**, 3677 (1997).
- [9] C. Schröter, B. El Marji, A. Lahmam-Bennani, A. Duguet, M. Lecas, and L. Spielberger, *J. Phys. B* **31**, 131 (1998).
- [10] I. Taouil, A. Lahmam-Bennani, A. Duguet, and L. Avaldi, *Phys. Rev. Lett.* **81**, 4600 (1998).
- [11] C. J. Joachain, *Quantum Collision Theory* (North-Holland, Amsterdam, 1975).
- [12] J. Berakdar, *Phys. Lett. A* **220**, 238 (1996).
- [13] J. Berakdar, *Phys. Rev. A* **55**, 1994 (1997).
- [14] A. W. Malcherek and J. S. Briggs, *J. Phys. B* **30**, 4419 (1997).
- [15] A. W. Malcherek, J.-M. Rost, and J. S. Briggs, *Phys. Rev. A* **55**, R3979 (1997).
- [16] M. Inokuti, *Rev. Mod. Phys.* **43**, 297 (1971).
- [17] A. Hylleraas, *Z. Phys.* **54**, 347 (1929).
- [18] J. Berakdar and H. Klar, *J. Phys. B* **26**, 4219 (1993).
- [19] F. Maulbetsch and J. S. Briggs, *J. Phys. B* **26**, 1679 (1993).
- [20] A. Huetz, P. Selles, D. Waymel, and J. Mazeau, *J. Phys. B* **24**, 1917 (1991).
- [21] Z. Teng and R. Shakeshaft, *Phys. Rev. A* **47**, R3487 (1993).